An empirical model to form and evolve galaxies in dark matter halos

2016 Res. Astron. Astrophys. 16 130

(http://iopscience.iop.org/1674-4527/16/8/013)

RAA 2016 Vol. **16** No. **8**, 130 (14pp) doi: 10.1088/1674–4527/16/8/130
http://www.raa-journal.org *http://iopscience.iop.org/raa*

***R**esearch in*
***A**stronomy and*
***A**strophysics*

An empirical model to form and evolve galaxies in dark matter halos

Shi-Jie Li[1,6], You-Cai Zhang[1], Xiao-Hu Yang[2,3], Hui-Yuan Wang[4], Dylan Tweed[2], Cheng-Ze Liu[2], Lei Yang[2], Feng Shi[1,6], Yi Lu[1], Wen-Tao Luo[1] and Jian-Wen Wei[5]

[1] Key Laboratory for Research in Galaxies and Cosmology, Shanghai Astronomical Observatory, Shanghai 200030, China; *sjli@shao.ac.cn*
[2] Center for Astronomy and Astrophysics, Shanghai Jiao Tong University, Shanghai 200240, China; *xyang@sjtu.edu.cn*
[3] IFSA Collaborative Innovation Center, Shanghai Jiao Tong University, Shanghai 200240, China
[4] Key Laboratory for Research in Galaxies and Cosmology, Department of Astronomy, University of Science and Technology of China, Hefei 230026, China
[5] Center for High Performance Computing, Shanghai Jiao Tong University, Shanghai 200240, China
[6] University of Chinese Academy of Sciences, Beijing 100049, China

Received 2016 March 21; accepted 2016 April 29

Abstract Based on the star formation histories of galaxies in halos with different masses, we develop an empirical model to grow galaxies in dark matter halos. This model has very few ingredients, any of which can be associated with observational data and thus be efficiently assessed. By applying this model to a very high resolution cosmological N-body simulation, we predict a number of galaxy properties that are a very good match to relevant observational data. Namely, for both centrals and satellites, the galaxy stellar mass functions up to redshift $z \simeq 4$ and the conditional stellar mass functions in the local universe are in good agreement with observations. In addition, the two point correlation function is well predicted in the different stellar mass ranges explored by our model. Furthermore, after applying stellar population synthesis models to our stellar composition as a function of redshift, we find that the luminosity functions in the ${}^{0.1}u$, ${}^{0.1}g$, ${}^{0.1}r$, ${}^{0.1}i$ and ${}^{0.1}z$ bands agree quite well with the SDSS observational results down to an absolute magnitude at about –17.0. The SDSS conditional luminosity function itself is predicted well. Finally, the cold gas is derived from the star formation rate to predict the HI gas mass within each mock galaxy. We find a remarkably good match to observed HI-to-stellar mass ratios. These features ensure that such galaxy/gas catalogs can be used to generate reliable mock redshift surveys.

Key words: cosmology: dark matter — galaxies: formation — galaxies: halos

1 INTRODUCTION

Galaxies are thought to form and evolve in cold dark matter (CDM) halos, however, our understandings of the galaxy formation mechanisms and the interaction between baryons and dark matter are still quite poor, especially quantitatively (see Mo et al. 2010, for a detailed review). Within hydrodynamic cosmological simulations, the evolution of the gas component is described on top of dark matter, with extensive implementation of cooling, star formation and feedback processes. Such detailed implementation of galaxy formation within a cosmological framework requires vast computational time and resources (Springel et al. 2005).

However, the formation of dark matter halos can be easily derived and interpreted, such that merger trees can be derived directly from N-body simulations, or through Monte Carlo methods. Within those trees, sub-grid models can be applied on the scale of dark matter halos themselves. Such models are referred to as semi-analytic models (hereafter SAMs), and provide the means to test galaxy formation models at a much lower computational cost (Cattaneo et al. 2007).

In SAMs, some simple equations describing the underlying physical ingredients regarding the accretion and cooling of gas, star formation, etc., are connected to the properties of a dark matter halo, so that baryons can evolve within the dark matter halo merger trees. The related free parameters in these equations are tuned to statistically match some physical properties of observed galaxies.

The basic principles of modern SAMs were first introduced by White & Frenk (1991). Subsequently, numerous authors participated in studies of such models and made great progress (e.g. Kauffmann et al. 1993; Mo et al. 1998; Somerville & Primack 1999; Cole et al. 2000; De Lucia et al. 2004; Kang et al. 2005; Croton et al. 2006; Bower et al. 2006; Monaco et al. 2007; Guo et al. 2011). Through using adjustable parameters, SAMs have reproduced many

statistical properties of large galaxy samples in the local universe such as luminosity functions (LFs), galactic stellar mass functions (SMFs), correlation functions, Tully-Fisher relations, metallicity-stellar mass relations, black hole-bulge mass relations and color-magnitude relations. However, the main shortcoming of SAMs is that there are too many free parameters and degeneracies. Despite the successes of these galaxy formation models, the sub-grid physics is still poorly understood (Benson 2012). By tuning the free parameters, the SAM prediction could match some of the observed galaxy properties in consideration, especially in the local universe. However, none of the current SAMs can match the low and high redshift data simultaneously (Somerville et al. 2012). Traditionally, parameters are preferably set without providing a clear statistical measure of success for a combination of observed galaxy properties.

As a SAM costs much less computation time than a full hydrodynamical galaxy formation simulation, one is allowed to explore a wide range of parameter space in an acceptable time interval. To better constrain the SAM parameters, the Monte Carlo Markov Chain (MCMC) method has been applied to SAMs in recent years. The first paper that incorporated MCMC into SAM is Kampakoglou et al. (2008), which used the star formation rate (SFR) and metallicity as a model constraint. Some other groups using SAM have also developed their own models associated with the MCMC method (e.g. Henriques et al. 2009, 2013; Benson & Bower 2010; Bower et al. 2010; Lu et al. 2011, 2012; Mutch et al. 2013). The details of MCMC are beyond the aims of this paper, and we refer the readers to relevant literature (Press et al. 2007; Trotta 2008).

As pointed out in Benson & Bower (2010), our understanding of galaxy formation is far from complete. SAMs should not be thought of as attempts to provide a final theory of galaxy formation, but instead to provide means by which new ideas and insights may be tested and by which quantitative and observationally comparable predictions may be extracted in order to test current theories. Because of the large number of free parameters, new ideas and insights relevant to sub-grid physics may often introduce new degeneracies with increased complexity and uncertainties to the model, either a traditional SAM or MCMC method. In general, if we take a step back from SAMs, we find that the largest part of the parameters and uncertainties are related to the sub-grid physics implemented for the gas. Focusing the model on the formation and evolution of the *stars* within dark matter halos, the vast majority of the uncertainties in SAM related to the gas component will be reduced.

Understanding the relation between dark matter halos and galaxies is a vital step to model galaxy formation and evolution in dark matter halos. In recent years, we have seen drastic progress in establishing the connection between galaxies and dark matter halos, such as the halo occupation distribution (HOD) models (e.g. Jing et al. 1998, Berlind & Weinberg 2002, Zehavi et al. 2005, Foucaud et al. 2010, Watson et al. 2011, Wake et al. 2012, Leauthaud et al. 2012), and the closely related conditional stellar mass (or luminosity) function models (Yang et al. 2003, van den Bosch et al. 2003, Conroy et al. 2006, van den Bosch et al. 2007, Yang et al. 2009, Yang et al. 2012, Rodríguez-Puebla et al. 2015). The former make use of the clustering of galaxies to constrain the probability of finding N galaxies in a halo with mass M. However, the latter make use of both clustering and luminosity (stellar mass) functions to constrain the probability of finding galaxies with given luminosity (or stellar mass) in a halo with mass M. In a recent study, Yang et al. (2012) (hereafter Y12) proposed a self-consistent model properly taking into account (1) the evolution of stellar-to-halo mass relation of central galaxies, and (2) the accretion and subsequent evolution of satellite galaxies. Based on the host halo and subhalo accretion models provided in Zhao et al. (2009) and Yang et al. (2011), Y12 obtained the conditional stellar mass functions (CSMFs) for both central and satellite galaxies as functions of redshift. Based on the mass assembly histories of central galaxies, the amount of accreted satellite galaxies and the fraction of surviving satellite galaxies constrained in Y12, we obtained the star formation histories (SFHs) of central galaxies in halos with different masses (Yang et al. 2013). Similar SFH models were also proposed based on N-body or Monte Carlo merger trees (e.g., Moster et al. 2013; Behroozi et al. 2013; Lu et al. 2014, hereafter Lu14). These SFH maps give us the opportunity to grow galaxies in N-body simulations without the need to model the complicated gas physics. In those models, referred to as empirical models (EMs) of galaxy formation, the growth of galaxies is statistically constrained using observational data.

This paper is organized as follows. In Section 2, we describe in detail our simulation data and EM model. In Section 3, we show our model predictions associated with the stellar masses of galaxies. The model predictions related to the luminosity and HI gas components are presented in Section 4. Finally, in Section 5, we provide our conclusions and discuss the applications of our model and the galaxy catalog thus constructed.

2 SIMULATION AND OUR EMPIRICAL MODEL

2.1 The Simulation

Similar to the SAMs, our EM also starts from dark matter halo merger trees. In this study, we use dark matter halo merger trees extracted from a high resolution N-body simulation. The simulation describes the evolution of the phase-space distribution of 3072^3 dark matter particles in a periodic box of $500\ h^{-1}\mathrm{Mpc}$ on a side. It was carried out in the Center for High Performance Computing, Shanghai Jiao Tong University. This simulation, hereby referred as L500, was run with `L-GADGET`, a memory-optimized version of `GADGET2` (Springel et al. 2005). The cosmological parameters adopted by this simulation are consistent with WMAP9 results as follows:

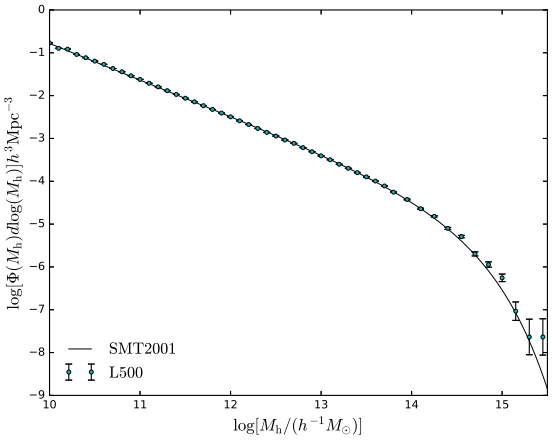

Fig. 1 Halo mass functions of the simulation. The black curve and cyan circles represent respectively the SMT2001 analytic prediction and data extracted from the L500 simulation.

$\Omega_{\rm m} = 0.282$, $\Omega_\Lambda = 0.718$, $\Omega_{\rm b} = 0.046$, $n_{\rm s} = 0.965$, $h = H_0/(100\,{\rm km\,s^{-1}\,Mpc^{-1}}) = 0.697$ and $\sigma_8 = 0.817$ (Hinshaw et al. 2013). The particle masses and softening lengths are, respectively, $3.3747 \times 10^8 h^{-1} M_\odot$ and $3.5h^{-1}{\rm kpc}$. The simulation is started at redshift 100 and has 100 outputs from $z = 19$, equally spaced in $\log(1+z)$.

Dark matter halos were first identified by the friends-of-friends (FOF) algorithm with linking length of 0.2 times the mean particle separation and containing at least 20 particles. The corresponding dark matter halo mass function of this simulation at redshift $z = 0$ is represented by cyan circles in Figure 1, while the black curve corresponds to the analytic model prediction by Sheth et al. (2001) (SMT2001). The halo mass function of this simulation is in good agreement with the analytic model prediction in the related mass ranges.

Based on halos at different outputs, halo merger trees were constructed (Lacey & Cole 1993). We first use the SUNFIND algorithm (Springel et al. 2001) to identify the bound substructures within the FOF halos or FOF groups. In an FOF group, the most massive substructure is defined as the main halo and the other substructures are defined as subhalos. Each particle contained in a given subhalo or the main halo is assigned a weight which decreases with the binding energy. We then find all main halos and subhalos in the subsequent snapshot that contains some of its particles. The descendant of any (sub)halo is chosen as the one with the highest weighted count of common particles. This criterion can be understood as a weighed maximum shared merit function (see Springel et al. 2005 for more details). Note that, for some small halos, the tracks of which are temporarily lost in the subsequent snapshot, we skip one snapshot in finding their descendants. These descendants are called "non-direct descendants."

2.2 The Empirical Model of Galaxy Formation

Unlike any SAM where each halo initially gets a lump of hot gas to be eventually turned into a galaxy (Baugh 2006), our EM starts with stars. Here we make use of the SFH map of dark matter halos obtained by Yang et al. (2013) to grow galaxies. In our EM of galaxy formation, *central* and *satellite* galaxies are assumed to be located at the centers of main halos and subhalos respectively. Their velocities are assigned using those of the main halos and subhalos. For those satellite galaxies whose subhalos are disrupted (e.g. orphan galaxies), the host halo is populated according to its NFW profile. Their velocities are assigned according to the halo velocity combined with the velocity dispersion (see Yang et al. 2004 for the details of such an assignment).

Apart from the obvious issue of positioning mock galaxies, we have to implement stellar mass evolution. For central and satellite galaxies, stellar mass $M_{\star,{\rm c}}(t_2)$ at a time t_2 is derived by adding to the stellar mass $M_{\star,{\rm c}}(t_1)$ at a time t_1 the contribution from star formation $\Delta M_{\star,{\rm c}}(t_1)$ and disrupted satellites $\Delta M_{\star,{\rm dis}}(t_1)$ as follows

$$M_\star(t_2) = M_\star(t_1) + \Delta M_\star(t_1,t_2) + \Delta M_{\star,{\rm dis}}(t_1,t_2)\,. \quad (1)$$

Obviously before implementing these models, the galaxies have to be seeded. For each halo and subhalo, we follow the merger tree back in time to determine the earliest time output (at $t_{\rm min}$) when it was identified as a halo (at least 20 particles). Then a seed galaxy with initial stellar mass $M_\star(t_{\rm min})$ is assigned to this halo at the beginning redshift. Here the stellar mass is assigned according to the central-host halo mass relation obtained by Yang et al. (2012), taking into account the cosmology of our simulations. We note that only halos with direct descendants are seeded.

2.2.1 *Star formation of central galaxies*

We first model the growth of *central* galaxies that are associated with the host (main) halos. Listed below are the details.

– In order to integrate the contribution of star formation between snapshots corresponding to times t_1 and $t_2 =$

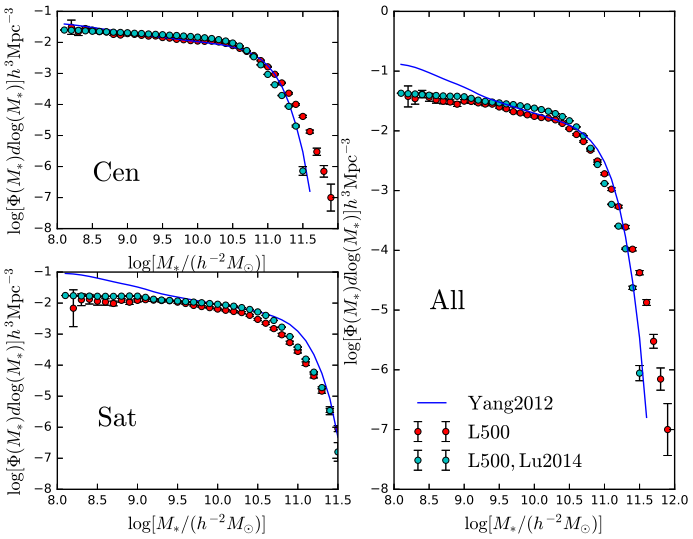

Fig. 2 The *upper left*, *lower left* and *right* panels show the galaxy SMFs for central, satellite and all galaxies, respectively. In each panel, the red filled circles with error bars are the galaxy SMF of SDSS DR7 obtained by Yang et al. (2012). The cyan circles with error bars are our fiducial EM results based on the L500 simulation. The blue curves are similar results but based on the SFH model of Lu14. The error bars of our EM are calculated using 500 bootstrap re-samplings.

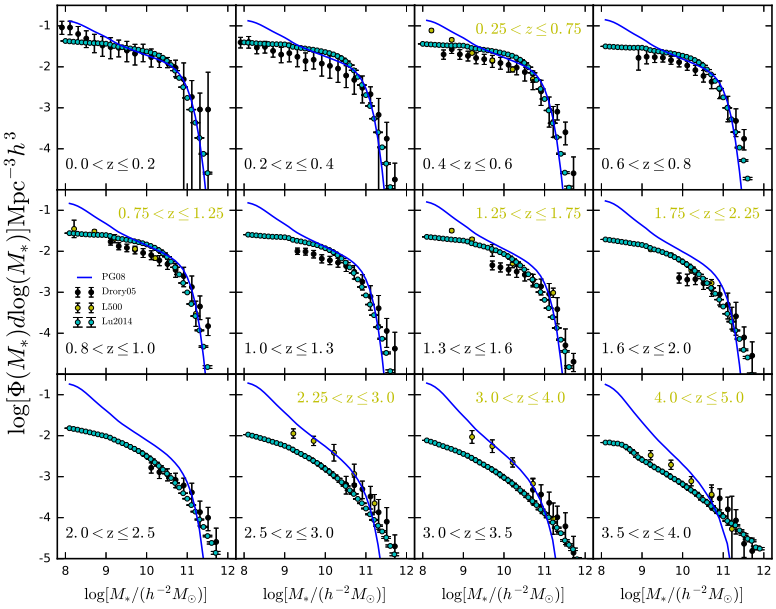

Fig. 3 SMF of galaxies at different redshift bins as indicated in each panel. In all panels we compare our EM prediction (*cyan filled circles*) and the Lu14 (*blue curve*) predictions applied to the L500 simulation to the Spitzer measurements (*black circles*) published in PG08. The redshift selection is indicated in black. We also add results obtained by Drory05, in similar redshift ranges (indicated in yellow for the relevant panels). The error bars of our EM are calculated using 500 bootstrap re-samplings.

$t_1 + \Delta T$, we increase the time resolution by defining smaller timesteps $\Delta t = \Delta T/N$. Here we choose $N = 5$, since greater values have very limited impact on the results. We also assume that the SFR is constant during any timestep Δt.

– Then we estimate $\dot{M}_\star(t)$, the SFR of a central galaxy at time t in a halo with mass M_h. As shown in Yang et al. (2013), the distributions of SFR of central galaxies have quite large scatters around the median values and show quite prominent bimodal features. To partly take into account these scatters, for each timestep Δt, the SFR $\dot{M}_\star(t)$ is drawn from a lognormal distribution with mean $\dot{M}_{\star,0}(t)$ and dispersion σ. So, the SFR of

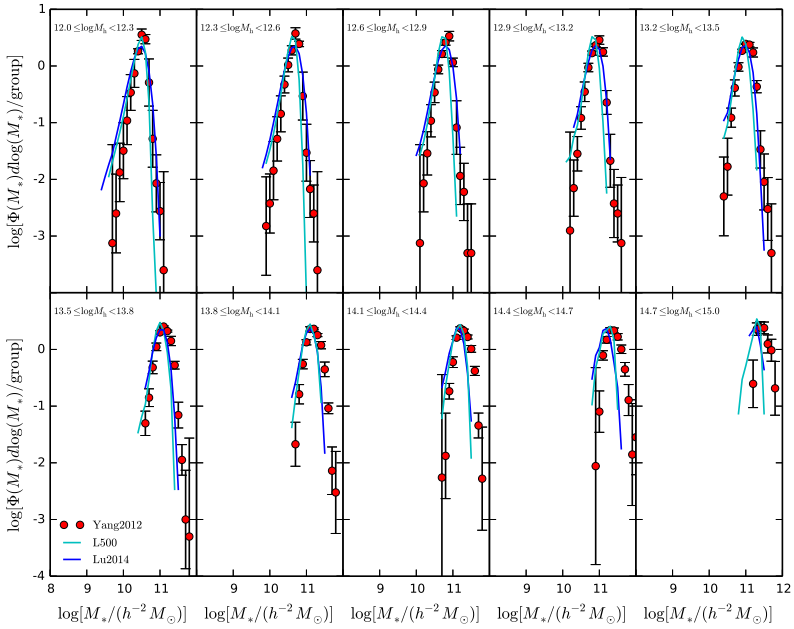

Fig. 4 CSMFs of central galaxies. Different panels correspond to different halo mass bins as indicated. The cyan curves are the CSMFs of our EM, while blue curves are obtained using the Lu14 SFH model. Red filled circles with error bars are the CSMFs of SDSS DR7 obtained by Yang et al. (2012).

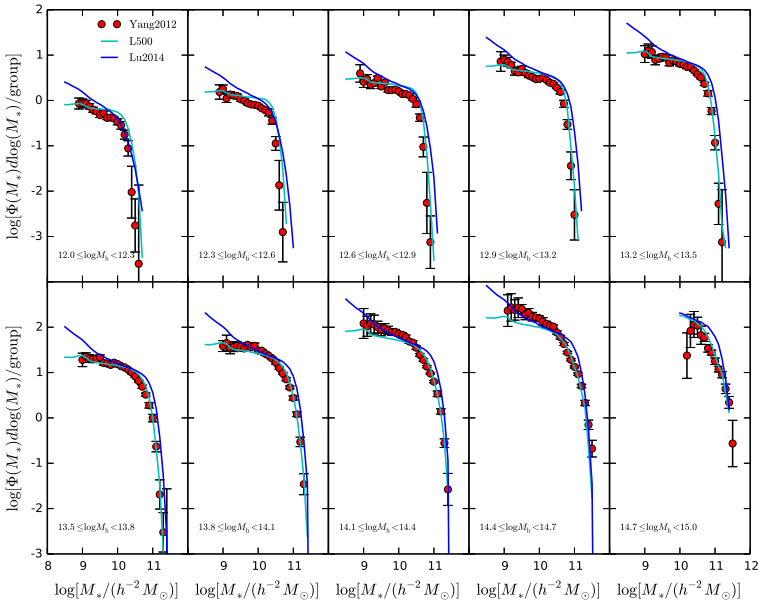

Fig. 5 Similar to Fig. 3 but for satellite galaxies.

central galaxies is indeed set as

$$\log \dot{M}_\star(t) = \log \dot{M}_{\star,0}(t) + \sigma \cdot N_{\rm gasdev}\,, \qquad (2)$$

where $\dot{M}_{\star,0}(t)$ is the median SFR predicted by Yang et al. (2013) and $N_{\rm gasdev}$ is a random number generated using code from Numerical Recipes (Press et al. 2007). Here we adopt a $\sigma = 0.3$ lognormal scatter as suggested in Yang et al. (2013).

– The stellar mass formed between the snapshots, $\Delta M_\star(t_1, t_2)$, is determined as

$$\Delta M_\star(t_1, t_2) = \sum_{t=t_1}^{t=t_2} \dot{M}_\star(t)\Delta t\,. \qquad (3)$$

2.2.2 Star formation in satellite galaxies

After focusing on the growth of central galaxies, we need to focus on the satellite galaxies. We start by modeling their growth while they are still associated with subhalos. Once the host halo enters a bigger one and becomes a subhalo, the SFR of the new satellite is expected to decline as a function of time due to the stripping effect and other causes. Here we use the star formation model of the satellite galaxy proposed by Lu14 to construct their SFH. A simple τ model has been adopted to describe the SFR decline in Lu14 as follows

$$\dot{M}_{\star,\rm sat}(t) = \dot{M}_{\star}(t_a) \exp\left(-\frac{t-t_a}{\tau_{\rm sat}}\right), \quad (4)$$

where t_a is the time when the galaxy is accreted into its host to become a satellite and $\dot{M}_{\star}(t_a)$ the corresponding SFR. $\tau_{\rm sat}$ is the exponential decay timescale characterizing the decline of the star formation for a galaxy with stellar mass $M_{\star}$. We adopt the following model of the characteristic time

$$\tau_{\rm sat} = \tau_{\rm sat,0} \exp\left(-\frac{M_{\star}}{M_{\star,\rm c}}\right), \quad (5)$$

where $\tau_{\rm sat,0}$ is the characteristic time for a galaxy with a stellar mass of $M_{\star,\rm c}$. The values $\tau_{\rm sat,0}$ and $M_{\star,\rm c}$ used in our model are the best fit values of MODEL III in Lu14 with $\log(H_0\tau_{\rm sat,0}) = -1.37$ and $\log M_{\star,\rm c} = -1.4$.

The growth of the satellite stellar mass thus becomes

$$\Delta M_{\star,\rm sat}(t_1,t_2) = \dot{M}_{\star}(t_a) \exp\left(-\frac{t_2-t_a}{\tau_{\rm sat}}\right) \cdot \Delta T \quad (6)$$

2.2.3 Merging and stripping of satellite galaxies

Apart from the *in situ* star formation, another important process in our model is the merging and stripping of satellite galaxies. The merging process has been studied by many people through hydrodynamical simulation (e.g. Zentner et al. 2005; Boylan-Kolchin et al. 2008; Jiang et al. 2008). Here we assume that the satellite galaxies orbiting within a dark matter halo may experience dynamical friction and will eventually be disrupted, and only a small fraction of stars finally merge with the central galaxy of the halo.

When a satellite cannot be associated with a subhalo, we use a delayed merger scheme where the satellite coalesces with the central after the dynamical friction timescale described in the fitting formula of Jiang et al. (2008)

$$T_{\rm dyn} = 1.4188 \frac{r_{\rm c} M_{\rm h}}{v_{\rm c} M_{\rm sub}} \frac{1}{\ln(1+\frac{M_{\rm h}}{M_{\rm sub}})}, \quad (7)$$

where $M_{\rm sub}$ and $M_{\rm h}$ are the respective *halo* masses associated with satellite and central galaxies, at the timestep a satellite galaxy was last found in a subhalo. This formula is valid for a small satellite with halo mass $M_{\rm sub}$ orbiting at radius $r_{\rm c}$ in a halo with circular velocity $v_{\rm c}$. As the satellite galaxy that was last found in a subhalo is disrupted after $\Delta t = T_{\rm dyn}$, we transfer a fraction of its stellar mass to the central galaxy. Hence, the contribution of the disrupted satellite follows

$$\Delta M_{\star,\rm dis}(t_1,t_2) = f_{\rm merger} \sum M_{\star,\rm sat}(t_{\rm sat}), \quad (8)$$

where $M_{\star,\rm sat}(t_{\rm sat})$ is the stellar mass of the in-falling satellite as determined when it was last found in a subhalo at $t_{\rm sat}$ with $t_{\rm sat} + T_{\rm dyn} \leq t_2$. $f_{\rm merger}$ is a fraction of the satellite galaxy stellar mass merged into the central galaxy. Here $f_{\rm merger} = 0.13$ is set to the best fit value of MODEL III in Lu14.

2.2.4 Passive evolution of galaxies

Finally, we take into account the passive evolution of both central and satellite galaxies. As we have the stellar mass composition of each galaxy as a function of time, the final stellar mass is determined as

$$\begin{aligned} M_{\star}(t_0) =& M_{\star}(t_{\rm min}) \cdot f_{\rm passive}(t_0 - t_{\rm min}) \\ &+ \sum_{t=t_{\rm min}}^{t=t_0} \Delta M_{\star}(t) \cdot f_{\rm passive}(t_0 - t), \end{aligned} \quad (9)$$

where $f_{\rm passive}(t)$ is the mass fraction of stars remaining at time t after the formation. We obtained $f_{\rm passive}(t)$ from Bruzual & Charlot (2003), courtesy of Stephane Charlot (private communication).

2.3 Other Star Formation History Models

There have been many other SFH models proposed in recent years (e.g. Conroy & Wechsler 2009, Behroozi et al. 2013). Here we make use of the model constrained by Lu14 in order to further test our EM. This model is similar in a sense that it consists of predicting SFR within halos and subhalos to build galaxies. In the mass property section of our results, the properties of the central and satellite galaxies are compared to our fiducial EM predictions.

Lu14 developed an empirical approach to describe the SFH model of central galaxies and satellite galaxies. They assumed an analytic formula for the SFH of central galaxies with a few free parameters. The galaxies grow in dark matter halos based on the halo merger trees generated by Extended Press-Schechter (EPS: Bond et al. 1991; Bower 1991) formalism and Monte Carlo method. With different observational constraints, they derived four different EMs. Here we only pick Model III in Lu14 to compare with our model. In Lu14, the SFR of central galaxies can be written as follows

$$\begin{aligned} \dot{M}_{\star} =& \mathcal{E} \frac{f_B M_{\rm vir}}{\tau_0} \Big(1+z\Big)^{\kappa} (X+1)^{\alpha} \\ &\times \Big(\frac{X+\mathcal{R}}{X+1}\Big)^{\beta} \Big(\frac{X}{X+\mathcal{R}}\Big)^{\gamma}, \end{aligned} \quad (10)$$

where $\mathcal{E}$ is an overall efficiency; f_B is the cosmic baryonic mass fraction; τ_0 is a dynamic timescale of the halos at

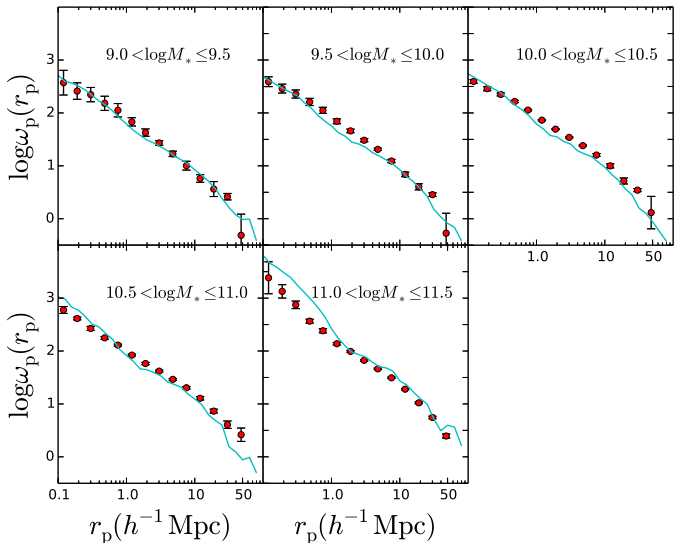

Fig. 6 Projected 2PCFs of galaxies in different stellar mass bins as indicated in each panel. Red filled circles with error bars are the 2PCFs of SDSS DR7 obtained by Yang et al. (2012) and cyan curves are our EM results.

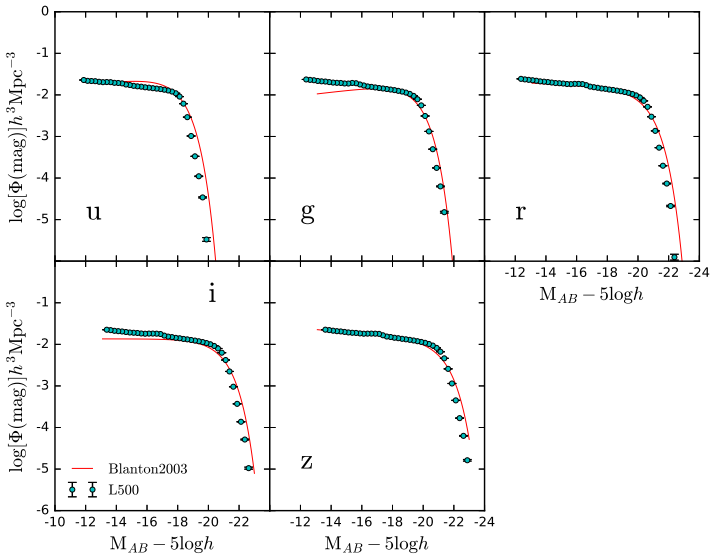

Fig. 7 LFs of galaxies in the u, g, r, i, z band at $z = 0.1$. The solid curve in each panel is the corresponding best fit Schechter LF obtained by Blanton et al. (2003) from SDSS DR1.

the present day, set to be $\tau_0 \equiv 1/(10H_0)$; and κ is fixed to be $3/2$ so that $\tau_0/(1+z)^{3/2}$ is roughly the dynamical timescale at redshift z. The quantity X is defined to be $X \equiv M_{\rm vir}/M_{\rm c}$, where $M_{\rm c}$ is a characteristic mass and $\mathcal{R}$ is a positive number that is smaller than 1. For the SFR of satellite galaxies, the related formula is already provided in Equation (4).

3 THE STELLAR MASS PROPERTIES OF GALAXIES

In order to check the performance of our EM for galaxy formation, we check the SMF and the two point correlation function (2PCF) of galaxies, and compare them to observational measurements. The related observational measurements are the SMFs at different redshifts (Yang et al. 2012; Pérez-González et al. 2008, hereafter PG08; Drory et al. 2005, hereafter Drory05), the CSMFs at low redshift (Yang et al. 2012) and the 2PCFs for galaxies in different stellar mass bins.

3.1 SMFs of Galaxies at Different Redshifts

The first set of observational measurements is the SMFs of galaxies at redshift $z = 0.0$ which are shown in Figure 2

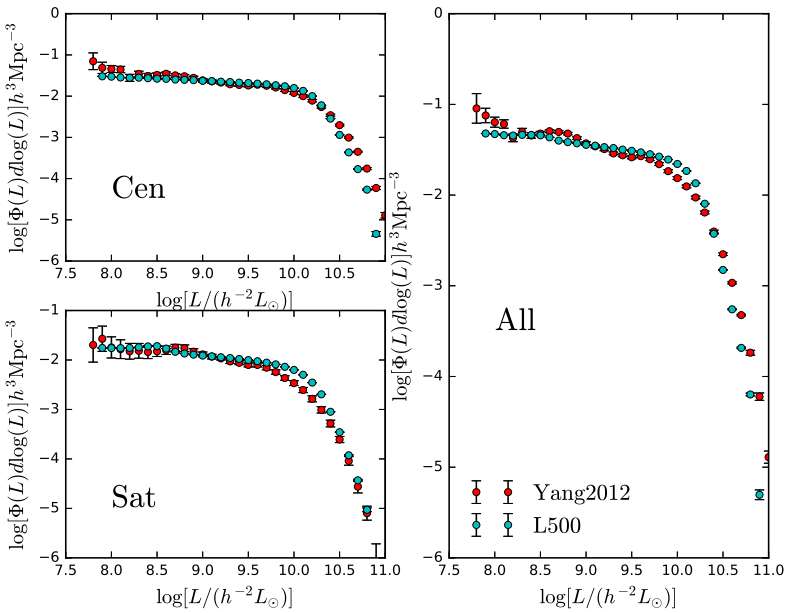

Fig. 8 LFs of central, satellite and all galaxies in the r band in the local universe. Here results are shown for observational measurements (*red dots*) and our fiducial model predictions (*cyan dots*).

for all (right panel), central (upper-left panel) and satellite (low-left panel) galaxies. The red circles with error bars indicate the observational data obtained from SDSS DR7 by Yang et al. (2012). Cyan circles with error bars are the results of our model applied to the halo merger trees of the L500 simulation. Meanwhile, blue curves are obtained using the Lu14 SFH model on the same trees.

From the upper-left panel of Figure 2, it is clear that for central galaxies the results of our model show an excellent agreement with observational data within a large stellar mass range ($\log M_* \sim 8.1-11.0$). However, in the high mass range ($\log M_* \gtrsim 11.0$), we somewhat underestimate the SMF. This discrepancy is probably caused by the fact that in our model, we used the median SFH to grow galaxies in dark matter halos. However in reality, scatter in SFHs with high mass central galaxies may be larger and depend on their large scale environment. In addition, in our model we did not take into account the major mergers of galaxies, where only the $f_{\rm merger} = 0.13$ portion of stripped satellite galaxies can be accreted to the central galaxies. For the SFH models of Lu14, the results are very similar to our fiducial ones.

For the satellite galaxies, as shown in the lower-left panel of Figure 2, our fiducial EM reproduces the overall SMFs quite well. However, a slight deviation (overprediction) is seen at the middle mass range ($\log M_* \sim 10.4 - 10.9$). In these satellite galaxies, either the SFH modeled by Equation (4) is somewhat too strong, or the stripping and disruption of a satellite modeled by Equation (7) is not efficient enough. As for the Lu14 model, it does not match that well with the SDSS observations, especially in the low mass range ($\log M_* \sim 8.0 - 9.5$). In the high mass range ($\log M_* \sim 11.0 - 11.5$), it overpredicts the mass function. Nevertheless, as the Lu14 model itself is intended to reproduce the much steeper slope of the LF at the faint end, especially for satellite galaxies, such differences are expected.

The right panel of Figure 2 shows the SMF of all galaxies which include central galaxies and satellite galaxies. The results of our fiducial EM in general agree with the observational data, with slight discrepancies at the high mass range ($\log M_* \gtrsim 11.0$) mainly contributed by centrals, and in the middle mass range ($\log M_* \sim 10.4-10.9$) mainly contributed by satellites. The Lu14 model shows a larger discrepancy at the low mass range ($\log M_* \sim 8.0 - 9.5$) which is caused by the satellite components.

Next, we check the SMFs of galaxies at higher redshifts. Shown in Figure 3 are SMFs of galaxies in different redshift bins as indicated in each panel. In these higher redshift bins, in order to mimic the typical error in the stellar mass estimation in observations, we add logarithmic scatters to the stellar masses of galaxies with values of $\sigma_c(z) = \max[0.173, 0.2z]$ (see Yang et al. 2012 for more details). The yellow filled circles with error bars are results obtained by Drory et al. (2005), in which they have combined the data from the FORS Deep Field and from the GOODS/CDFS Field. The cyan circles with error bars are our EM results based on the L500 simulation, while blue curves are the results of the Lu14 model based on the L500 simulation.

As shown in Figure 3, in both low and high redshift bins $z < 1.0$ and $z > 2.0$, the SMFs from our model agree quite well with the observational results. However, in the redshift range $1.0 < z < 2.0$, our model overpredicts the SMFs.

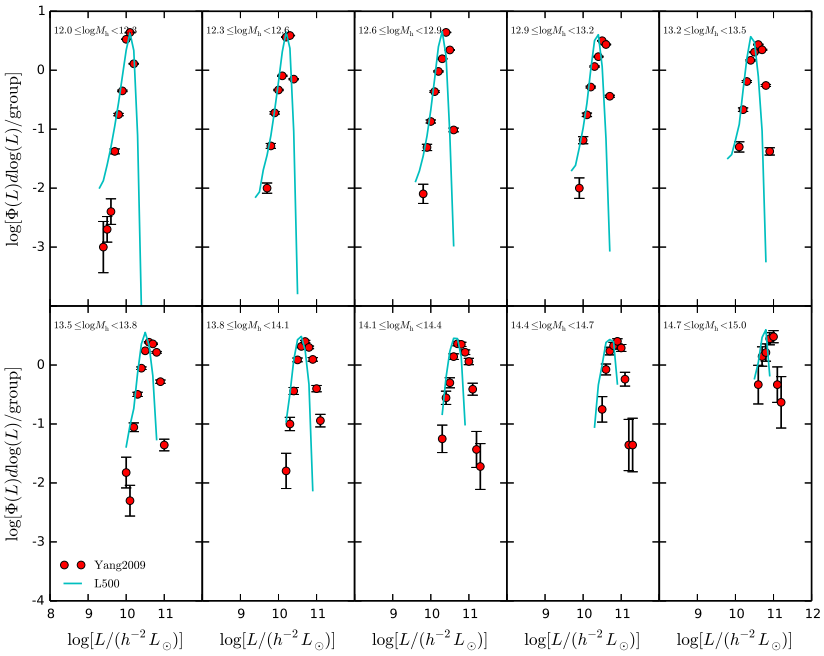

Fig. 9 CLFs of central galaxies in halos with different mass bins. Here results are shown for observational measurements (*red dots*) and our fiducial model predictions (*cyan curves*).

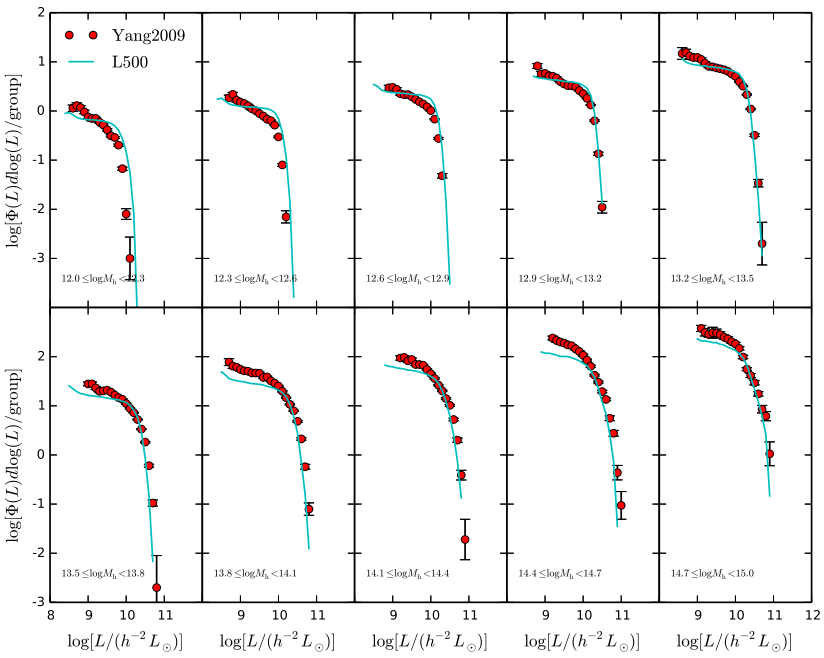

Fig. 10 Similar to Fig. 9 but for the satellite galaxies.

As seen in the lower-left panel of Figure 2, this discrepancy might be due to some overprediction of satellite galaxy counts. For comparison, we also show results based on the Lu14 model, which present even higher SMFs within the redshift range $1.0 < z < 2.0$.

3.2 CSMFs of Galaxies at $z = 0$

The CSMF $\phi(M_*|M_{\rm h})$, which describes the average number of galaxies as a function of galaxy stellar mass M_* that can be formed within halos of mass $M_{\rm h}$, is an impor-

tant measure that can be used to constrain galaxy formation models. As carried out in Liu et al. (2010) using the CSMFs of satellite galaxies, classical semi-analytical models at that time typically overpredicted the satellite components by a factor of two which indicates that either less (or smaller) satellites can be formed, or more satellite galaxies need to be disrupted. Here we compare our model predictions with observational data in Figure 4 and Figure 5 for central and satellite galaxies separately.

Based on the SDSS DR7 galaxy group catalog, Yang et al. (2012) obtained the CSMFs of central galaxies and satellite galaxies, which are shown as the red filled circles with error bars in Figure 4 and Figure 5, respectively. The CSMFs from our model are shown as cyan solid curves. Blue curves are the CSMFs obtained from galaxy catalogs constructed using the Lu14 model.

As shown in Figure 4, the central galaxy CSMFs of our model and the Lu14 model are very similar. Both of them agree well with the observations in halo mass range $12.0 \leq \log M_{\rm h} < 13.8$ but are slightly underestimated in halo mass range $13.8 \leq \log M_{\rm h} < 15.0$. As shown in Figure 5 for satellite galaxies, the CSMFs of our model agree well with the observations in general. There are small deviations in halo mass ranges $12.0 \leq \log M_{\rm h} < 12.3$, $12.3 \leq \log M_{\rm h} < 12.6$ and $12.6 \leq \log M_{\rm h} < 12.9$. In these ranges, our model overestimates the CSMFs at $9.5 \leq \log M_* < 10.5$. Thus, the overpredicted satellite galaxies shown in Figure 2 are mainly in these Milky Way sized and group sized halos. While in the Lu14 model, as seen for the satellite galaxy SMF shown in Figure 2, the CSMFs in halos with different masses all show an upturn at the low mass end.

3.3 2PCFs of Galaxies

The 2PCF which measures the excess of galaxy pairs as a function of distance is a widely used quantity to describe the clustering properties of galaxies. In terms of galaxy formation, it can be used to constrain the HOD of galaxies (Jing et al. 1998) and to constrain the conditional luminosity function (CLF) of galaxies (Yang et al. 2003). Here we compare the model predictions of 2PCFs in our galaxy catalogs to observations.

Figure 6 shows the projected 2PCFs of galaxies in different stellar mass bins. Our model predictions are shown as the solid curves , and the observational data obtained by Yang et al. (2012) from SDSS DR7 are shown as the filled circles with error bars. Our overall model predictions show quite a good match with the observations in the stellar mass range $9.0 < \log M_* < 11.0$. However, in the most massive stellar mass bin ($11.0 < \log M_* < 11.5$), our model result is higher than the observations for $r_{\rm p} \lesssim 1h^{-1}{\rm Mpc}$. The too strong clustering at $r_{\rm p} < 1\ h^{-1}{\rm Mpc}$ for these high mass objects is mainly caused by the fact that due to the insufficient prediction of the central galaxies, the satellite fraction in this mass bin is overpredicted (see Fig. 2).

4 THE LUMINOSITY AND GAS PROPERTIES OF GALAXIES

Apart from the stellar masses of galaxies, we now turn to the luminosity and gas components of galaxies.

4.1 Luminosities of Galaxies in Different Bands

As detailed in Section 2.2, from the halo merger histories derived from the L500 simulation, we model galaxies from an estimation of their sellar mass and SFR as a function of time. We use this information to predict the photometric properties of our model galaxies using the stellar population synthesis model of Bruzual & Charlot (2003) that incorporates a Salpeter IMF (Salpeter 1955). Since our model does not include the gas component in galaxies, we cannot directly trace the chemical evolution of the stellar population. To circumvent this problem, we follow the metallicity - stellar mass relation derived in Lu14 from observations of galaxies at all redshifts *in a specified range*. We adopt the mean relation based on the data of Gallazzi et al. (2005), which can roughly be described as

$$\log_{10} Z \ = \ \log_{10} Z_\odot + \frac{1}{\pi} \tan\left[\frac{\log_{10}(M_\star/10^{10} M_\odot)}{0.4}\right] -0.3\,. \quad (11)$$

This observational relation extends down to a stellar mass of $10^9 M_\odot$ and has a scatter of $0.2\,{\rm dex}$ at the massive end and of $0.5\,{\rm dex}$ at the low mass end.

Using the stellar population synthesis model, we can obtain galaxy luminosities in different bands. In Figure 7, we show the LFs of all galaxies in the five different SDSS bands (u, g, r, i, z) at $z = 0.1$. For comparison, we also show the corresponding best fit of the Schechter luminosity functions (LFs) obtained by Blanton et al. (2003) from SDSS DR1 in each panel. The observational measurements and corresponding model fittings are roughly limited to the absolute magnitude limit $(-16, -16.5, -17, -17.5, -18)$ in (u, g, r, i, z) bands, respectively. Within these magnitude limits, our model predictions agree with the observational data fairly well with very slight underpredictions at the bright ends. Only in the u-band do we see a prominent deficit of galaxies at ${}^{0.1}{\rm M}_u - 5\log h \sim -16.0$. These behaviors indicate that the stellar compositions as a function of time, as derived with our model, are on average accurate.

In addition to the LFs of the full galaxy population, we can distinguish the contribution from the centrals and the satellites.

Figure 8 shows the r band LFs of all (right panel), central (upper-left panel) and satellite (lower-left panel) galaxies. Our fiducial model predictions are shown as the cyan dots with error bars obtained from 500 bootstrap resamplings. Red points with error bars are obtained by Yang et al. (2009) but were updated to SDSS DR7. Similar to Figure 2, our model underestimates the central galaxy LF at the high luminosity end ($10.5 \lesssim \log L \lesssim 11.0$) and overestimates the satellite galaxy LF in the luminosity range ($10.0 \lesssim \log L \lesssim 10.5$).

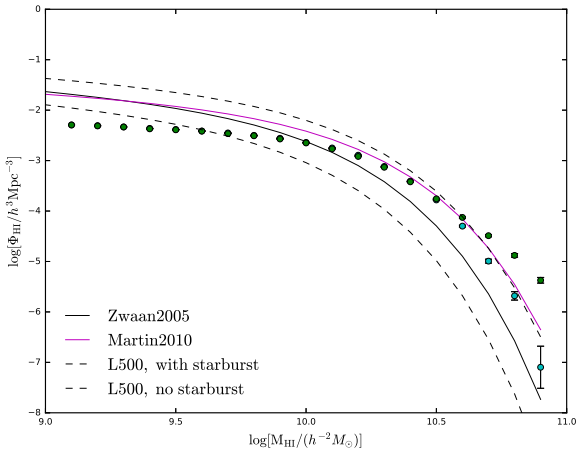

Fig. 11 The HI mass functions: *green dots* are our fiducial model predictions, while *cyan dots* are the model predictions that take into account the starburst. The *black solid line* shows the best fit observational results obtained by Zwaan et al. (2005) with *dashed lines* that indicate the associated $\pm 1\sigma$ scatter. The magenta curve is the observational fitting formula obtained by Martin et al. (2010).

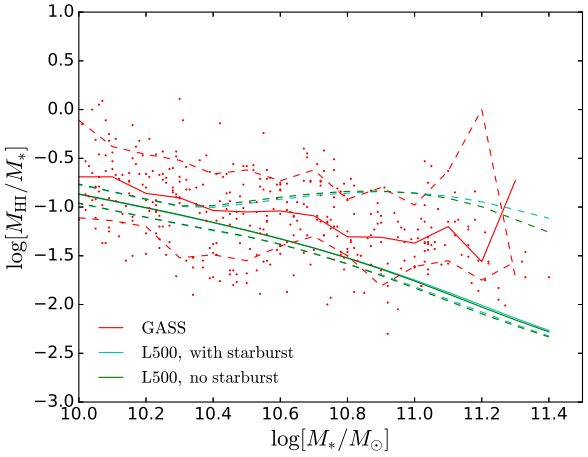

Fig. 12 The HI-to-stellar mass ratios as a function of galaxy stellar mass. Here red points are data from the GASS (Catinella et al. 2013) compilation. Red curves are the median (*solid*) and 68% confidence range (*dashed*) of the ratio in the GASS sample. Green and cyan curves represent the median (*solid*) and 68% confidence range (*dashed*) of our fiducial and starburst model predictions, respectively.

Similarly to the CSMFs, the CLFs describe, as a function of luminosity L, the average number of galaxies that reside in a dark matter halo with a given mass M_h.

In Figure 9 the CLFs obtained from our mock catalogs are compared to the observational measurements obtained by Yang et al. (2009) (also updated to SDSS DR7). As one could expect, the performance of CLFs associated with central galaxies is quite similar to the situation found for the CSMFs in Figure 4. The central galaxy CLFs of our model agree well with the observational results in the $12.0 \leq \log M_{\rm h} < 13.5$ halo mass range, although still there is some discrepancy for $13.5 \leq \log M_{\rm h} < 15.0$.

As for the satellite galaxies shown in Figure 10, the situation is somewhat different with respect to the CSMFs. Our model matches well with observations in $12.9 \leq \log M_{\rm h} < 13.8$, but underestimates the number of satellite galaxies at the low luminosity end in high mass halos $13.8 \leq \log M_{\rm h} < 15.0$. These discrepancies are highly interesting as they differ from the one we found for the CSMFs (Fig. 5), as it indicates that the colors of these galaxies are not entirely properly modeled.

4.2 HI Masses of Galaxies

Although our EM is limited to model the star components of galaxies, we can estimate the gas components within the galaxies. Here we focus on the cold gas that is associated with star formation (Schmidt 1959). The star formation law most widely implemented in SAM was proposed by Kennicutt (1998) as follows

$$\Sigma_{\rm SFR} = (2.5 \pm 0.7) \times 10^{-4} \times \left(\frac{\Sigma_{\rm gas}}{1\ M_\odot {\rm pc}^{-2}}\right)^{1.4\pm0.15} M_\odot\ {\rm yr}^{-1}\ {\rm kpc}^{-2}\,, \quad (12)$$

where $\Sigma_{\rm SFR}$ and $\Sigma_{\rm gas}$ are the surface densities of star formation and gas, respectively.

In this paper, we use the model proposed in Fu et al. (2010) to estimate the cold gas within our galaxies. This method consists of following the build-up of stars and gas within a fixed set of 30 radial "rings." The radius of each ring is given by the geometric series

$$r_i \;=\; 0.5\times 1.2^i [h^{-1}\,{\rm kpc}] \qquad (i=1,2...30)\,. \quad (13)$$

According to Mo et al. (1998), the cold gas is distributed exponentially with surface density profile

$$\Sigma_{\rm gas}(r) \;=\; \Sigma^0_{\rm gas}\exp(-r/r_{\rm d})\,, \quad (14)$$

where $r_{\rm d}$ is the scale length of the galaxy and $\Sigma^0_{\rm gas}$ is given by $\Sigma^0_{\rm gas}=m_{\rm gas}/(2\pi r_{\rm d}^2)$.

With the above ingredients, we are able to predict the total amount of cold gas associated with each galaxy. However, observationally, we only have a relatively good estimate of the HI mass in the local universe. Here we calculate HI masses associated with galaxies by assuming a constant $\rm H_2/HI$ ratio of 0.4 and a hydrogen mass fraction $X=0.74$ (Lagos et al. 2011; Baugh et al. 2004; Power et al. 2010).

Figure 11 shows the HI mass function of galaxies in the local universe obtained from our mock galaxy catalog (green dots). For comparison, in Figure 11 we also show, using a black curve, the fitting formula of the HI mass function obtained by Zwaan et al. (2005) from HIPASS

$$\Theta(M_{\rm HI})dM_{\rm HI} \;=\; \Big(\frac{M_{\rm HI}}{M^*_{\rm HI}}\Big)^{\alpha}\exp\Big(-\frac{M_{\rm HI}}{M^*_{\rm HI}}\Big) \times d\Big(\frac{M_{\rm HI}}{M^*_{\rm HI}}\Big)\,, \quad (15)$$

where $\alpha=-1.37\pm0.03$ and $\log(M^*_{\rm HI})/\,M_\odot=9.80\pm0.03h_{75}^{-2}$. Black dashed lines indicate the $\pm1\sigma$ scatter. An additional observational HI mass function is obtained by Martin et al. (2010) using the $1/V_{\rm max}$ method (magenta curve).

Our model only shows a fair agreement with these observational data, even though it underpredicts the HI mass function at $\log M_{\rm HI}\lesssim 9.6$ and overpredicts the HI mass function at $\log M_{\rm HI}\gtrsim 10.5$. These discrepancies are possibly caused by different factors. The first one is, of course, the uncertainties in the SFR-cold gas mass ratios. In addition to this, as the SFRs in low mass halos have much larger scatters than the ones we implement here (see fig. 1 in Yang et al. (2013)), adopting a larger scatter may help to solve the HI mass function deficiency at the low mass end. On the massive end of the HI mass function, the difference may be connected to starburst galaxies (with high SFR). However, in reality, a starburst is not necessarily associated with the largest cold gas component. Luo et al. (2014) have checked the morphologies of starburst galaxies which are defined as having SFRs five times higher than the median for a given stellar mass. They found that more than half of them are associated with gas rich major mergers. To partly take this into account, we adopt the collisional starburst model proposed by Somerville et al. (2001) used in many SAMs (Somerville et al. 2008; Guo et al. 2011). During the starburst process, the increased stellar mass of the central galaxy is

$$\delta m_{\rm starburst} \;=\; (m_{\rm gas,\,sat}+m_{\rm gas,\,cen}) \times e_{\rm burst}\left(\frac{m_{\rm sat}}{m_{\rm cen}}\right)^{\gamma_{\rm burst}}\,, \quad (16)$$

where $m_{\rm gas,\,cen}$ ($m_{\rm gas,\,sat}$) is the cold gas mass of the central (satellite) galaxy, and $m_{\rm cen}$ ($m_{\rm sat}$) is the sum of stellar mass and cold gas mass of the central (satellite) galaxy, $e_{\rm burst}=0.55$ and $\gamma_{\rm burst}=0.69$. The values of $e_{\rm burst}$ and $\gamma_{\rm burst}$ are determined from isolated galaxy merger simulations performed by Cox et al. (2008). Within our merger trees, we identify these starburst galaxies and swap their SFRs with the highest ones in a halo with similar mass. The cold gas for these galaxies is updated using Equation (16).

In Figure 11 using cyan dots, we show how this starburst implementation successfully corrects the overestimation of HI mass function at the massive end.

Apart from the HI mass functions, we also compare the HI-to-stellar mass ratios of galaxies. Figure 12 illustrates the HI-to-stellar mass ratio $\log[M_{\rm HI}/M_*]$ as a function of galaxy stellar mass. Red points are from the GASS compilation (Catinella et al. 2013) while the red curve represents the median value and red dashed curves indicate the $16^{\rm th}$ and $84^{\rm th}$ percentile ranges of $\log[M_{\rm HI}/M_*]$. The green solid and dashed curves represent the median and $16^{\rm th}$ and $84^{\rm th}$ percentile ranges of our fiducial model prediction from the L500 simulation respectively. In addition, the cyan curves are obtained from the starburst variation of the model. We can see that both our models reproduce the average trends of HI-to-stellar mass ratios as a function of stellar mass quite well. However, the scatter of the model prediction is smaller than the observation at low masses. We think that this may be caused by the relation between the SFR and cold gas used in our model.

5 SUMMARY

Based on the SFHs of galaxies in halos with different masses derived by Yang et al. (2013), we use an EM to study galaxy formation and evolution. Compared to traditional SAMs, this model has fewer free parameters, each of which can be associated with the observational data. Applying this model to merger trees derived from N-body simulations, we predict several galaxy properties that agree well with observational data. Our main results can be summarized as follows.

(1) At redshift $z=0$, the SMFs of all galaxies agree well with observations within $8.0<\log M_*<11.3$ but our estimate is slightly low in the high stellar mass end ($11.3<\log M_*<12.0$).
(2) Our SMFs generally show a fair agreement with the observational data at higher redshifts up to 4. However

in redshift $1.0 < z < 2.0$, the SMFs at the low mass end are somewhat overestimated.

(3) At redshift $z = 0$, the CSMFs of central galaxies agree well with observations in the $12.0 \leq \log M_{\rm h} < 13.8$ halo mass range, but are somewhat shifted to lower masses in halo mass range $13.8 \leq \log M_{\rm h} < 15.0$. In addition, the CSMFs of satellite galaxies agree quite well with observations.

(4) The projected 2PCFs in different stellar mass bins calculated from our fiducial galaxy catalog can match the observations well. Only in the most massive stellar mass bin is the correlation overpredicted at small scales.

(5) We can derive LFs from our model in the ${}^{0.1}u$, ${}^{0.1}g$, ${}^{0.1}r$, ${}^{0.1}i$ and ${}^{0.1}z$ bands. They prove to be roughly consistent with the SDSS observational results obtained by Blanton et al. (2003).

(6) The central galaxy CLFs of our model agree well with the observational results in the halo mass range $12.0 \leq \log M_{\rm h} < 13.5$, quite similar to the SMFs. However, the satellite galaxy CLFs are somewhat underestimated at the faint end in halos with mass $12.9 \leq \log M_{\rm h} < 13.8$.

(7) Our prediction of HI mass function agrees with the observational data at roughly the $\pm 1\sigma$ level at $\log M_{\rm HI} \gtrsim 9.6$, but is somewhat underestimated at lower mass ends.

Our model predictions are roughly consistent, but not perfect, in terms of stellar mass, luminosity and HI mass components of galaxies. Such a method is a potential tool to study galaxy formation and evolution as an alternative to SAMs or abundance matching methods. The galaxy and gas catalogs that have been compiled can be used to construct redshift surveys for future deep surveys.

Acknowledgements This work is supported by the 973 Program (No. 2015CB857002), the National Natural Science Foundation of China (Grant Nos. 11203054, 11128306, 11121062, 11233005, 11073017 and 11421303), NCET-11-0879, the Strategic Priority Research Program "The Emergence of Cosmological Structures" of the Chinese Academy of Sciences, Grant No. XDB09000000 and the Shanghai Committee of Science and Technology, China (Grant No. 12ZR1452800). SJL thanks Ming Li for his help in dealing with the simulation data, Ting Xiao for her useful discussion concerning HI gas and Jun Yin for her help in stellar population synthesis modeling.

A computing facility award on the PI cluster at Shanghai Jiao Tong University is acknowledged. This work is also supported by the High Performance Computing Resource in the Core Facility for Advanced Research Computing at Shanghai Astronomical Observatory.

References

Baugh, C. M. 2006, Reports on Progress in Physics, 69, 3101
Baugh, C. M., Croton, D. J., Gaztañaga, E., et al. 2004, MNRAS, 351, L44
Behroozi, P. S., Wechsler, R. H., & Conroy, C. 2013, ApJ, 770, 57
Benson, A. J. 2012, New Astron., 17, 175
Benson, A. J., & Bower, R. 2010, MNRAS, 405, 1573
Berlind, A. A., & Weinberg, D. H. 2002, ApJ, 575, 587
Blanton, M. R., Hogg, D. W., Bahcall, N. A., et al. 2003, ApJ, 592, 819
Bond, J. R., Cole, S., Efstathiou, G., & Kaiser, N. 1991, ApJ, 379, 440
Bower, R. G. 1991, MNRAS, 248, 332
Bower, R. G., Benson, A. J., Malbon, R., et al. 2006, MNRAS, 370, 645
Bower, R. G., Vernon, I., Goldstein, M., et al. 2010, MNRAS, 407, 2017
Boylan-Kolchin, M., Ma, C.-P., & Quataert, E. 2008, MNRAS, 383, 93
Bruzual, G., & Charlot, S. 2003, MNRAS, 344, 1000
Catinella, B., Schiminovich, D., Cortese, L., et al. 2013, MNRAS, 436, 34
Cattaneo, A., Blaizot, J., Weinberg, D. H., et al. 2007, MNRAS, 377, 63
Cole, S., Lacey, C. G., Baugh, C. M., & Frenk, C. S. 2000, MNRAS, 319, 168
Conroy, C., & Wechsler, R. H. 2009, ApJ, 696, 620
Conroy, C., Wechsler, R. H., & Kravtsov, A. V. 2006, ApJ, 647, 201
Cox, T. J., Jonsson, P., Somerville, R. S., Primack, J. R., & Dekel, A. 2008, MNRAS, 384, 386
Croton, D. J., Springel, V., White, S. D. M., et al. 2006, MNRAS, 365, 11
De Lucia, G., Kauffmann, G., Springel, V., et al. 2004, MNRAS, 348, 333
Drory, N., Salvato, M., Gabasch, A., et al. 2005, ApJ, 619, L131
Foucaud, S., Conselice, C. J., Hartley, W. G., et al. 2010, MNRAS, 406, 147
Fu, J., Guo, Q., Kauffmann, G., & Krumholz, M. R. 2010, MNRAS, 409, 515
Gallazzi, A., Charlot, S., Brinchmann, J., White, S. D. M., & Tremonti, C. A. 2005, MNRAS, 362, 41
Guo, Q., White, S., Boylan-Kolchin, M., et al. 2011, MNRAS, 413, 101
Henriques, B. M. B., Thomas, P. A., Oliver, S., & Roseboom, I. 2009, MNRAS, 396, 535
Henriques, B. M. B., White, S. D. M., Thomas, P. A., et al. 2013, MNRAS, 431, 3373
Hinshaw, G., Larson, D., Komatsu, E., et al. 2013, ApJS, 208, 19
Jiang, C. Y., Jing, Y. P., Faltenbacher, A., Lin, W. P., & Li, C. 2008, ApJ, 675, 1095

Jing, Y. P., Mo, H. J., & Börner, G. 1998, ApJ, 494, 1
Kampakoglou, M., Trotta, R., & Silk, J. 2008, MNRAS, 384, 1414
Kang, X., Jing, Y. P., Mo, H. J., & Börner, G. 2005, ApJ, 631, 21
Kauffmann, G., White, S. D. M., & Guiderdoni, B. 1993, MNRAS, 264, 201
Kennicutt, Jr., R. C. 1998, ApJ, 498, 541
Lacey, C., & Cole, S. 1993, MNRAS, 262, 627
Lagos, C. D. P., Lacey, C. G., Baugh, C. M., Bower, R. G., & Benson, A. J. 2011, MNRAS, 416, 1566
Leauthaud, A., Tinker, J., Bundy, K., et al. 2012, ApJ, 744, 159
Liu, L., Yang, X., Mo, H. J., van den Bosch, F. C., & Springel, V. 2010, ApJ, 712, 734
Lu, Y., Mo, H. J., Katz, N., & Weinberg, M. D. 2012, MNRAS, 421, 1779
Lu, Y., Mo, H. J., Weinberg, M. D., & Katz, N. 2011, MNRAS, 416, 1949
Lu, Z., Mo, H. J., Lu, Y., et al. 2014, MNRAS, 439, 1294
Luo, W., Yang, X., & Zhang, Y. 2014, ApJ, 789, L16
Martin, A. M., Papastergis, E., Giovanelli, R., et al. 2010, ApJ, 723, 1359
Mo, H. J., Mao, S., & White, S. D. M. 1998, MNRAS, 295, 319
Mo, H., van den Bosch, F. C., & White, S. 2010, Galaxy Formation and Evolution (Cambridge, UK: Cambridge University Press)
Monaco, P., Fontanot, F., & Taffoni, G. 2007, MNRAS, 375, 1189
Moster, B. P., Naab, T., & White, S. D. M. 2013, MNRAS, 428, 3121
Mutch, S. J., Poole, G. B., & Croton, D. J. 2013, MNRAS, 428, 2001
Pérez-González, P. G., Rieke, G. H., Villar, V., et al. 2008, ApJ, 675, 234
Power, C., Baugh, C. M., & Lacey, C. G. 2010, MNRAS, 406, 43
Press, W. H., Teukolsky, S. A., Vetterling, W. T., & Flannery, B. P. 2007, Numerical Recipes in C++ : The Art of Scientific Computing (3rd edn.; Cambridge University Press)
Rodríguez-Puebla, A., Avila-Reese, V., Yang, X., et al. 2015, ApJ, 799, 130
Salpeter, E. E. 1955, ApJ, 121, 161
Schmidt, M. 1959, ApJ, 129, 243
Sheth, R. K., Mo, H. J., & Tormen, G. 2001, MNRAS, 323, 1
Somerville, R. S., Gilmore, R. C., Primack, J. R., & Domínguez, A. 2012, MNRAS, 423, 1992
Somerville, R. S., Hopkins, P. F., Cox, T. J., Robertson, B. E., & Hernquist, L. 2008, MNRAS, 391, 481
Somerville, R. S., & Primack, J. R. 1999, MNRAS, 310, 1087
Somerville, R. S., Primack, J. R., & Faber, S. M. 2001, MNRAS, 320, 504
Springel, V., White, S. D. M., Tormen, G., & Kauffmann, G. 2001, MNRAS, 328, 726
Springel, V., White, S. D. M., Jenkins, A., et al. 2005, Nature, 435, 629
Trotta, R. 2008, Contemporary Physics, 49, 71
van den Bosch, F. C., Yang, X., & Mo, H. J. 2003, MNRAS, 340, 771
van den Bosch, F. C., Yang, X., Mo, H. J., et al. 2007, MNRAS, 376, 841
Wake, D. A., van Dokkum, P. G., & Franx, M. 2012, ApJ, 751, L44
Watson, D. F., Berlind, A. A., & Zentner, A. R. 2011, ApJ, 738, 22
White, S. D. M., & Frenk, C. S. 1991, ApJ, 379, 52
Yang, X., Mo, H. J., Jing, Y. P., van den Bosch, F. C., & Chu, Y. 2004, MNRAS, 350, 1153
Yang, X., Mo, H. J., & van den Bosch, F. C. 2003, MNRAS, 339, 1057
Yang, X., Mo, H. J., & van den Bosch, F. C. 2009, ApJ, 695, 900
Yang, X., Mo, H. J., van den Bosch, F. C., et al. 2013, ApJ, 770, 115
Yang, X., Mo, H. J., van den Bosch, F. C., Zhang, Y., & Han, J. 2012, ApJ, 752, 41
Yang, X., Mo, H. J., Zhang, Y., & van den Bosch, F. C. 2011, ApJ, 741, 13
Zehavi, I., Zheng, Z., Weinberg, D. H., et al. 2005, ApJ, 630, 1
Zentner, A. R., Berlind, A. A., Bullock, J. S., Kravtsov, A. V., & Wechsler, R. H. 2005, ApJ, 624, 505
Zhao, D. H., Jing, Y. P., Mo, H. J., & Börner, G. 2009, ApJ, 707, 354
Zwaan, M. A., Meyer, M. J., Staveley-Smith, L., & Webster, R. L. 2005, MNRAS, 359, L30